Electrostatic Probe Measurements in Argon Plasma Boundary Layer

By

Kazuoki MATSUOKA,* Haruaki KISHIGE,* Michio NISHIDA,**
and Goro KAMIMOTO,**

(Received September 25, 1976)

Abstract

A combined experimental and numerical investigation was conducted in a partially ionized boundary layer flow on a flat plate. The experiments were carried out in a low-density plasma wind tunnel, with argon as the test gas at the local freestream Mach number of 4.4. A cylindrical Langmuir probe was used to measure the ion number density and the electron temperature in the boundary layer.

The effect of flush probe size, bias and flow properties were examined. Numerical calculations were made by using the charged species conservation and electron energy equations in the quasineutral region of the boundary layer, except for a thin plasma sheath.

Numerical profiles of the ion number density and the electron temperature agreed fairly well with the experimental results. Also, ambipolar diffusion fluxes theoretically predicted agreed very well with the flush probe ion saturation current measured by a flush probe.

1. Introduction

As is well known, the hypersonic re-entry of a space shuttle into the earth's atmosphere is the source of a great number of physical and thermo-chemical interacting phenomena. One of the important observables dealt with in this context is the charged particle number density.

A number of diagnostic techniques and instruments have been employed to

* Nara Technical College (Dr. Matsuoka was studying at Kyoto University as a visiting researcher during April 1967-March 1969 and April 1975-March 1976.)
** Department of Aeronautical Engineering.

measure the ion number density and density profiles. This ranges from microwave interferometry to optical spectrometry, and from radiation scattering techniques to electrostatic probes. Among others, the electrostatic probe, by virtue of its simplicity, became one of the most popular plasma diagnostic instruments. During the last few years, the flush-mounted electrostatic probe has been widely used to obtain information concerning the free stream charged particle properties.

Tseng et al.[1] performed the measurements in the boundary layer of a sharp flat plate located in the inviscid-core flow of a Mach 2.2 argon flow in a low-density plasma tunnel. The ambipolar diffusion fluxes predicted theoretically agreed very well with the measured flush probe ion saturation current. The validity of employing such a flush-mounted electrostatic probe in determining the free stream charged particle density was then established. But, in order to obtain the charged particle number density, the measured electron temperature profile was used. Boyer[2] performed the numerical and experimental studies to determine the current collection characteristics of flush-mounted electrostatic probes on a sharp flarp flat plate in an ionized hypersonic flow using a shock tunnel.

Lederman et al.[3] also performed the experimental investigation of flush-mounted probes in a pressure driven shock tube and a hypersonic pressure driven shock tunnel. In most of the work reported and known to the authors, the questions of what constitutes ion saturation, the effect of increasing bias, the effect of geometry and orientation of the probes and the effect of size on current collections have not been sufficiently explored.

In this paper, the electron temperature and ion number density profiles in the flat plate boundary layer were measured by the cylindrical Langmuir probe, and compared with the theory developed for the collisionless sheath consideration. Detailed information was obtained about the flush probe size effects and the prediction of the ion number densities at the outer edge of the boundary layer.

2. Notations

A	area
c	mass fraction of electron-ion pairs, $(\rho_I+\rho_{II})/\rho$
D_a	ambipolar diffusion coe ffcient
$\hat{E}$	energy given to electron gas per recombination
e	electronic charge
f	dimensionless stream function
h	static enthalpy
J	ion current density
k	Boltzmann constant

L	energy transfer rate due to inelastic collision
l	Chapman-Rubesin number, $\rho\mu/\rho_e\mu_e$
l_s	sheath thickness
M	Mach number
m	mass
n	number density
Pr	Prandtl number, $\mu c_p/\lambda$
Q_{ij}	cross section of collision between i- and j- species
R	energy transfer rate due to elastic collision
Re	Reynolds number, $\rho ux/\mu$
r_p	probe radius
Sc_a	ambipolar Schmidt number, $\mu/\rho D_a$
T	temperature
V_d	diffusion velocity
$\langle V_E \rangle$	mean electron velocity
V_I	mean ion velocity at sheath edge
V_p	probe potential
u	x-component of flow velocity
v	y-component of flow velocity
$\dot{W}$	mass production rate of electron-ion pairs
z	dimensionless mass fraction of electron-ion pairs
β	recombination coe ffcient
ε	$(m_E/m_A)^{1/2}$
η	transformed co-ordinate
Θ	dimensionless electron temperature
θ	dimensionless heavy particle temperature
λ	thermal conductivity
μ	viscosity
ξ	transformed co-ordinate
ρ	mass density
τ	T_{Ee}/T_{Ae}
ϕ	electric potential
$\bar{\chi}$	hypersonic viscous interaction parameter
ψ	stream function

Subscripts

A	atom
E	electron
e	boundary layer edge

I	ion
sh	sheath edge
w	wall
∞	free stream

3. Theoretical Consideration

3.1 Basic Equations

We consider the nonequilibrium laminar boundary layer on a flat plate in a partially ionized gas which is easily realized in a low density plasma. Therefore, we make the following assumptions:

(1) The gas is composed of argon atoms, ions and electrons.
(2) The degree of ionization $\ll 1$.
(3) There are no external magnetic and electric fields in the flow.
(4) The ions are in thermal equilibrium with the atoms everywhere, $T_A=T_I$.
(5) $u_A=u_I=u_E\equiv u$.
(6) Steady flow, $\partial/\partial t=0$.
(7) Collisionless sheath.
(8) Ambipolar diffusion.

Under the assumption (2), the over-all conservation equations are not coupled with the basic equations for the charged species, so that the basic equations to be solved here are the electron-ion conservation and electron energy equations. When we use the co-ordinate system as shown in Fig. 1, the basic equations are written as follows:

Conservation of electron-ion pairs:

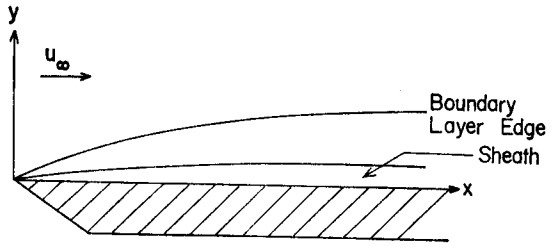

Fig. 1. Co-ordinate System.

$$\rho u\frac{\partial c}{\partial x}+\rho v\frac{\partial c}{\partial y}=\frac{\partial}{\partial y}\left(\rho D_a\frac{\partial c}{\partial y}\right)+\dot{W}. \tag{1}$$

Conservation of electron energy:

$$\frac{\partial}{\partial x}\left(\frac{3}{2}n_E kuT_E\right)+\frac{\partial}{\partial y}\left(\frac{3}{2}n_E kvT_E\right)=\frac{\partial}{\partial y}\left(\lambda_E\frac{\partial T_E}{\partial y}-\rho c_E V_{dE}h_E\right)$$
$$-n_E kT_E\left(\frac{\partial u}{\partial x}+\frac{\partial v}{\partial y}\right)+R+L. \tag{2}$$

When the electron-electron and electron-ion collisions predominate over the electron-atom collisions, R and λ_E are, respectively, of the form:[4]

$$R=12\sqrt{2}\,n_E^2\left(\frac{m_E kT_E}{\pi}\right)^{1/2}\frac{k(T_A-T_E)Q_{EE}}{m_A}, \tag{3}$$

$$\lambda_E=\frac{75k}{64(1+\sqrt{2})Q_{EE}}\left(\frac{\pi kT_E}{m_E}\right)^{1/2}. \tag{4}$$

since $Q_{EI}=Q_{EE}$ when $T_E/m_E \gg T_I/m_I$, Q_{EE} is expressed as

$$Q_{EE}=\frac{\pi e^4 \log\Lambda}{2(kT_E)^2}, \tag{5}$$

where $\Lambda=3(k^3T_E^3/m_E)^{1/2}/2e^3$.[5]

Now, $\dot{W}$ in Eq. (1) is the mass production rate of the electron-ion pairs. Under the condition considered here, further ionization in the boundary layer is negligible compared with the recombination of a pre-ionized gas, so that $\dot{W}$ is expressed as

$$\dot{W}=-\beta m_I n_E^2. \tag{6}$$

Using Chen's results[6], we make an approximate expression for the recombination coefficient of argon over the range 1000K $\leq T_E \leq$ 4000K and $10^{11}\mathrm{cm}^{-3} \leq n_E \leq 10^{14}\mathrm{cm}^{-3}$. It can be expressed by the double series:

$$\log_{10}\beta=\sum_{i=0}^{3}\sum_{j=0}^{2}A_{ij}\left(\log_{10}\frac{n_E}{10^{11}}\right)^i\left(\frac{1000}{T_E}\right)^{j/2}. \tag{7}$$

This procedure is the same as done by Talbot et al.[7] for hydrogen. Solving the resulting matrix equation, we have

$A_{00}=-12.88$, $A_{01}=2.074$, $A_{02}=-1.337$,
$A_{10}=-2.874$, $A_{11}=9.133$, $A_{12}=-5.259$,
$A_{20}=-1.160$, $A_{21}=-2.681$, $A_{22}=1.521$,
$A_{30}=-0.1536$, $A_{31}=0.3513$, $A_{32}=-0.1977$.

L is expressed as

$$L=\beta n_E^2 \hat{E}. \tag{8}$$

For an optically thin argon plasma, Chen[8] calculated $\hat{E}$. According to his result, $\hat{E}$ can be expressed approximately as

$$\hat{E}=\frac{2}{3}\left(\frac{n_E}{10^{13}}-0.1\right)+0.9 \text{ (in eV)}. \tag{9}$$

3.2 Boundary Conditions

The boundary conditions at the wall for the electron temperature and the mass fraction of the electron-ion pairs are determined as follows:[9]

For the present problem, where the wall is at a floating potential, the net current

density normal to the wall is zero. Hence, we have

$$n_{Esh}e\frac{\langle V_E\rangle}{4}\exp\left\{-\frac{e(\phi_{sh}-\phi_w)}{kT_{Esh}}\right\}-n_{Ish}eV_I=0. \tag{10}$$

Next, a relation is obtained from the continuity of the mass flow of the ions at the edge of the sheath and therefore

$$\left(\rho D_a\frac{\partial c}{\partial y}\right)_{sh}=\rho_{sh}c_{sh}V_I. \tag{11}$$

A third relation is obtained from the continuity of electron energy flux through the outer edge of the sheath and therefore

$$\left(\lambda_E\frac{\partial T_E}{\partial y}\right)_{sh}-(\rho c_E V_{dE}h_E)_{sh}=\{2kT_{Esh}+e(\phi_{sh}-\phi_w)\}$$
$$\times\frac{n_{Esh}}{4}\langle V_E\rangle\exp\left\{-\frac{e(\phi_{sh}-\phi_w)}{kT_{Esh}}\right\}, \tag{12}$$

where $\langle V_E\rangle=(8kT_{Esh}/\pi m_E)^{1/2}$ and $V_I=(kT_{Esh}/m_I)^{1/2}$. Since the sheath is very thin compared with the boundary layer thickness, these boundary conditions may be taken to be the boundary conditions at the wall.

The boundary conditions at the boundary layer edge are

$$c(\infty)=c_e,\quad T_E(\infty)=T_{Ee}. \tag{13}$$

It is well known that the development of a viscous boundary layer near the surface of the plate serves to generate a shock wave in the flow field. Over the length of the inserts, the value of a hypersonic viscous interaction parameter, $\bar{\chi}=M^3_\infty/\sqrt{Re_\infty}$, ranged from 2 to 3. Therefore, it is an intermediate interaction region. The flow properties at the outer edge of the boundary layer can be obtained using the weak and strong interaction theory.

3.3 Co-ordinate Transformation

In order to obtain a similar solution, the following transformation of co-ordinate is introduced:

$$\xi(x)=x,\quad \eta(x,y)=\left(\frac{u_e}{\rho_e\mu_e\xi}\right)^{1/2}\int_0^y\rho dy. \tag{14}$$

The over-all continuity equation is identically satisfied if we define a stream function ψ such tion $\partial\psi/\partial y=\rho u$ can $\partial\psi/\partial x=-\rho v$. By definig the dimensionless stream function $f=\psi/(\rho_e\mu_e u_e\xi)^{1/2}$, $\partial f/\partial\eta=u/u_e$ can be easily obtained. The following dimensionles quantities are introduced:

$$\theta=\frac{T_A}{T_{Ae}},\quad z=\frac{c}{c_e},\quad \theta=\frac{T_E}{T_{Ee}}. \tag{15}$$

Assuming a local similarity, the conservation equations (1) and (2) are rewritten as follows:

Conservation of electron-ion pairs:

$$\left(\frac{l}{Sc_a}z'\right)'+\frac{1}{2}fz'=-\xi\frac{n_{Ee}}{u_e}\beta_e\left(f'-\frac{z^2}{\theta}\frac{\beta}{\beta_e}\right). \tag{16}$$

servation of electron energy:

$$\Theta''+\left(\frac{5}{2}\frac{\Theta'}{\Theta}-\frac{\theta'}{\theta}+\frac{a}{2}\frac{z\theta f}{\Theta^{5/2}}\right)\Theta'+\frac{a}{3}\frac{\theta f}{\Theta^{5/2}}\left(\frac{3}{2}z'+\frac{z\theta'}{\theta}\right)\Theta$$
$$+b\xi\frac{z^2}{\Theta^4}\left(\frac{\theta}{\tau}-\Theta\right)+b\xi\left(1-\frac{1}{\tau}\right)\frac{\beta}{\beta_e}\frac{z}{\theta}=0. \tag{17}$$

here ξ is treated as a parameter, ( )' denotes the derivative with respect to η. The constants a and b are given by

$$a=\frac{3(1+\sqrt{2})}{5}Prc_e\frac{\varepsilon}{\tau^{1/2}}\frac{Q_{EEe}}{Q_{AAe}}, \tag{18}$$

$$b=\frac{256(2+\sqrt{2})}{25\pi}\frac{\mu_e}{\rho_e u_e}(\varepsilon Q_{EEe}n_{Ee})^2, \tag{19}$$

where Sc_a is the ambipolar Schmidt number expressed as[10]

$$Sc_a=\frac{2.51}{1+T_E/T_A}\frac{T_A+11.5T_a^{1/2}}{T_A+142}. \tag{20}$$

In Eq. (17) the diffusive heat flux is neglected since it is very small compared with the conductive heat flux.

The boundary conditions for z and Θ are rewritten as

$$z'(0)=Sc_a(0)Re_e^{1/2}\frac{V_I}{u_e}\frac{1}{\theta^{0.816}}z(0), \tag{21}$$

$$\Theta'(0)=\frac{64(1+\sqrt{2})}{75\pi}\left\{-\frac{1}{2}-\frac{1}{2}\log_e(2\pi)-\log_e\varepsilon\right\}$$
$$\times\left(\frac{\mu_e}{\rho_e u_e}\right)^{1/2}\varepsilon n_{Ee}Q_{EEe}\,\xi^{1/2}\frac{z(0)}{\Theta(0)}, \tag{22}$$

$$z(\infty)=1,\quad \Theta(\infty)=1, \tag{23}$$

where a relation $\mu\propto T^{0.816}$ for argon has been used.

4. Numerical Calculations

In order to compare the measured profiles with the theoretical ones, the profiles of the electron temperature and the ion number density have been numerically calculated. For the purpose of simplicity, $Pr=2/3$ and $l=1$ have been taken. Since both Eqs. (16) and (17) are coupled and nonlinear, iteration procedures are necessary to solve them. First, we can obtain the solutions of f and θ by solving the overall basic equations These solutions are used in Eqs. (16) and (17). In the second stage, by taking $Sc_a=1$ and neglecting the mass production term in Eq. (16), an

analytical solution of z can be easily obtained, which corresponds to a chemically frozen solution. Using this solution in Eq. (17), an approximate solution of Θ can be determined. Using the solutions of Θ in Eq. (17), the new approximate solutions of z can be obtained. Thus, the iterations are carried out. All computations using the Runge-Kutta-Gill method have been performed on the digital computer FACOM 230-75 at the Computer Center of Kyoto University.

5. Experimental Apparatus and Work

Experiments have been performed in a low-density plasma wind tunnel as shown in Fig. 2. A detailed description of this test facility and its associated instrumentation have been already reported.[11] The argon test gas is expanded through a hypersonic nozzle into a test section. The diameters of a nozzle throat and exit are 13.6 mm and 50 mm, respectively. The flat plate model is shown in Fig. 3, which is made of brass with a sharp leading edge of an angle 22°. It has a span of 120 mm, a length of 200 mm and a thickness of 20 mm, and is electrically insulated from the wall of the wind tunnel. The flat plate was water-cooled, and a thermocouple installed in the flat plate supervised the constancy of the surface temperature of the flat plate. Seven sets of inserts were employed to investigate the effect of probe size on the flush probe current collection. These seven inserts with different sizes of flush-mounted probes could be fitted into the groove with a 30 mm width on the master plate. Each insert is composed of six circular flush-mounted electrostatic probes with the same size, and these probes were arranged at 20 mm interval along the centerline.

The flush probes were made of a copper rod and insulated from the insert plate body by using heat-resisting bakelite. The dimensions of these flush probes are

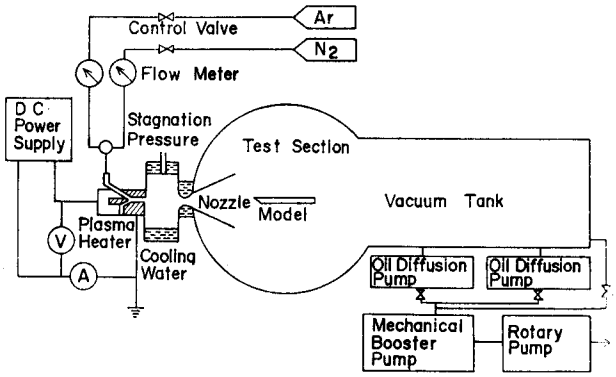

Fig. 2. Schematic of a Plasma Wind Tunnel.

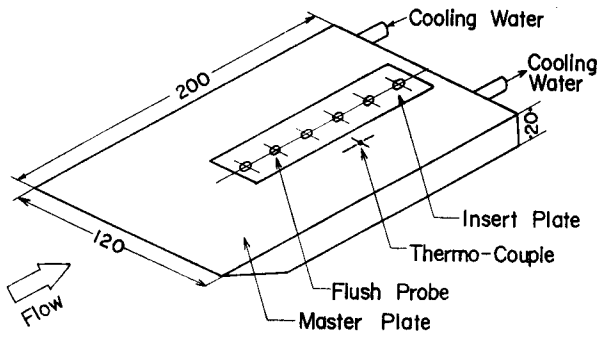

Fig. 3. Flat Plate Model.

listed in Table 1. The insert plates could be exchanged by loosening the split-lock mechanism. When the insert plates were installed in the master plate, they were flush with the flat plate surface and placed on the nozzle centerline. The flush probe and cylindrical probe measurements in argon were performed at six stations behind the leading edge. Figure 4 shows the configuration of the experimental apparatus.

Table 1 Sizes of Flush-Mounted Electrostatic Probes.

Nominal Diameter (cm)	Measured Radius (cm)
1.5	0.748
1.0	0.502
0.5	0.253
0.3	0.147
0.2	0.098
0.1	0.052
0.05	0.024

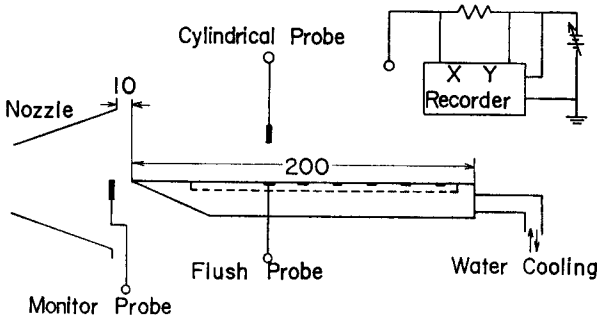

Fig. 4. Configuratisn of Experimental Apparatus.

Throughout the experiments, a single constant-voltage thin-wire probe was positioned at the nozzle exit to monitor a steady plasma flow. The typical flow conditions in the test section are summarized in Table 2. The electron temperature and ion number density profile measurements in the boundary layer were made by means of a cylindrical probe with a 0.30 mm diameter and a 12.4 mm length. The voltage applied to the flush probes was swept from -10.0 to 2 volts.

Table 2 Experimental Conditions

Argon Mass Flow Rate (gr/sec)			0.10
Stagnation Pressure (mmHg)			7.6
Pressure in Test Section (mmHg)			0.12
Mach Number, M_∞			4.4
Degree of Ionization			0.91×10^{-3}
$n_{A\infty}$ (cm^{-3})	1.2×10^{15}	Re_∞ (1. cm)	45
$n_{I\infty}$ (cm^{-3})	1.1×10^{12}	u_∞ (cm/sec)	1.7×10^{5}
$T_{A\infty}$ (K)	420	T_{Aw} (K)	320
$T_{E\infty}$ (K)	2500		

6. Experimental Results and Discussion

The probe measurements in the boundary layer were made from the freestream to about 1 mm above the flat plate surface. Measured electron temperature profiles at 80 mm and 180 mm from the leading edge of the flat plate are shown in Figs. 5 and 6, on which the results of the flush probe measurements are also represented.

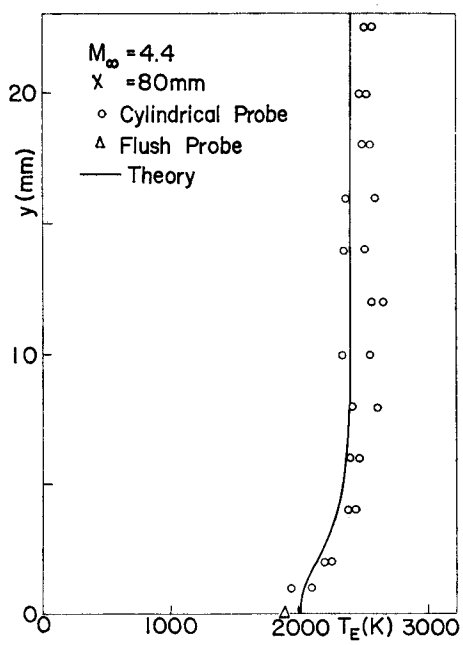

Fig. 5. Electron Temperature Profile. at x=80mm

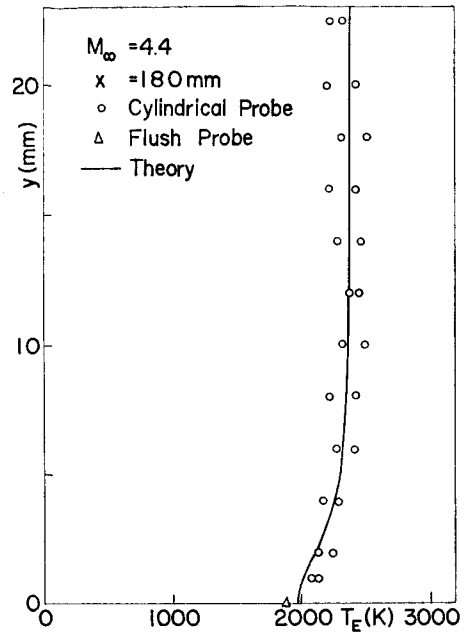

Fig. 6. Electron Temperature profile. at x=180mm

The experimental results are in good agreement with the calculated ones. The measured profiles display a decrease in T_{tr} of about 15% of the free stream value towards the flat plate surface. Boundary layer ion number density profiles obtained by means of the cylindrical probe are shown in Figs. 7 and 8. It is of interest to note that the ion number density at the flat plate surface is not negligibly small. Hence, it is suggested that the wall catalytic reaction rate constant is a finite rate. The measured ion number densities in the boundary layer are considerably larger than the calculated ones for a recombining flow. However, the calculated and measured ion number density profiles are qualitatively in good agreement. Previous to

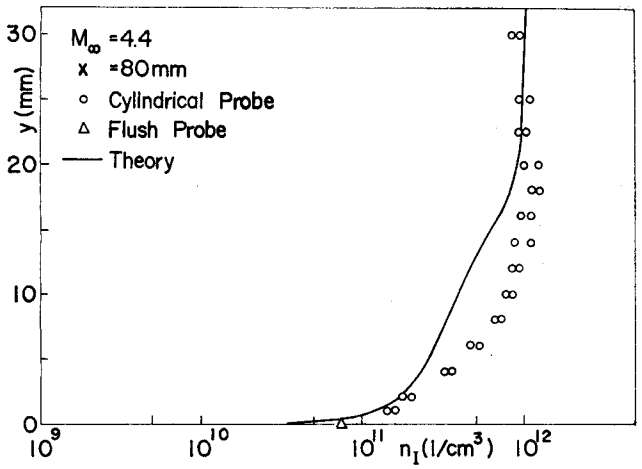

Fig. 7. Ion Number Density Profile at x=80mm

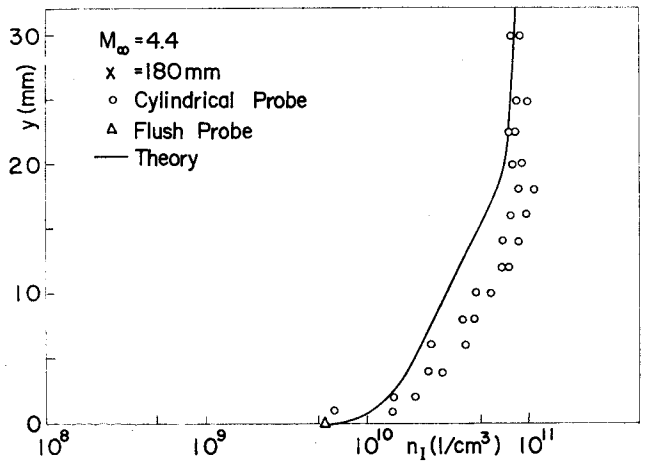

Fig. 8. Ion Number Density Profile at x=180mm

the experiments, the effect of the arrangement of the flush probe on the ion current collection had been investigated.

Figure 9 shows the constancy of the saturation ion current collection with respect to the bias potential for 15 mm and 0.5 mm diameter flush probes. For the large-sized flush probes (i. e. 15 mm diameter), it has been seen that the saturation ion current traces are essentially constant with respect to the biased potential. For the small-sized flush probes, the ion current is a very strong function of the biased potential since the effective collection area of small flush probes increases drastically with potential. The effects of the sheath fringing field on the ion current collection to smaller-sized flush probes are shown in Figs. 10 and 11, where the normalized current J/J_{ref} is plotted against the r_p/l_s ratio. All ion current densities were taken at -2 volts and were normalized by the reference diffusion flux to the flush probe ($r_p=7.5$ mm). It is seen that the current density can increase by a factor of 10 or more if l_s/r_p is rather large. The sheath thickness l_s is determined as follows:[12]

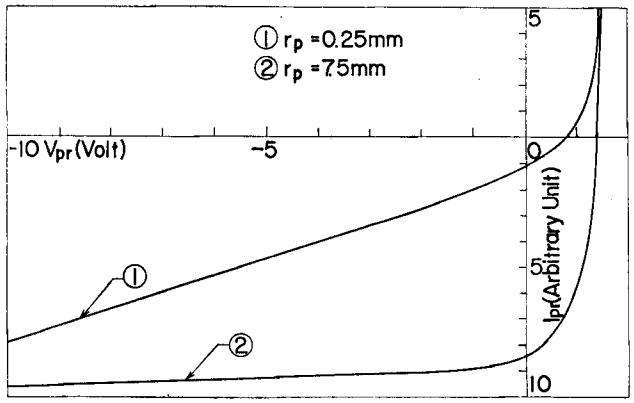

Fig. 9. Size Effect on Flush Prrobe Characteristics for $r_p=0.25$mm and $r_p=7.5$mm at x=80mm.

$$l_s=3.31\times10^2T_e^{-1/2}\lambda_D|V_p|^{3/4}. \tag{24}$$

If all the ions crossing this segment of a sphere are eventually collected by the probe, then the ratio of the effective collection area to the actual flush probe area, A_{eff}/A_p, becomes:

$$\frac{A_{eff}}{A_p}=1+\left(\frac{l_s}{r_p}\right)^2=\frac{J}{J_{ref}}. \tag{25}$$

Eq. (25) can be easily obtained from an integration of the segment of a sphere. It is of interest to note that the above equation is realized in the stationary plasma.

Calculated results using Eq. (25) are also shown in Figs. 10 and 11, and appear to agree well with experimental data.

Figure 12 shows the size effect on the flush probe ion current collection. The current density increases as the probe size decreases in agreement with the observations of Tseng et al.,[1] and Boyer et al.[2] The studies of Tseng et al. as well as the present studies have been performed under collisionless conditions and the results are interpreted in terms of a free-fall sheath thickness $l_s \propto |V_p|^{3/4}$. For the collisional thick sheath, the calculations of Boyer et al. indicate $l_s \propto |V_p|^{1/2}$.

Figure 13 shows the comparison of the experimental and theoretical ion current

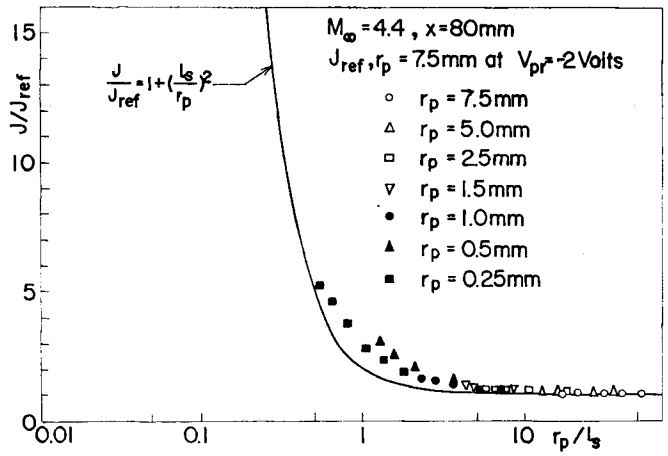

Fig. 10. Size Effect on Flush Probe Ion Current Collection at x=80mm.

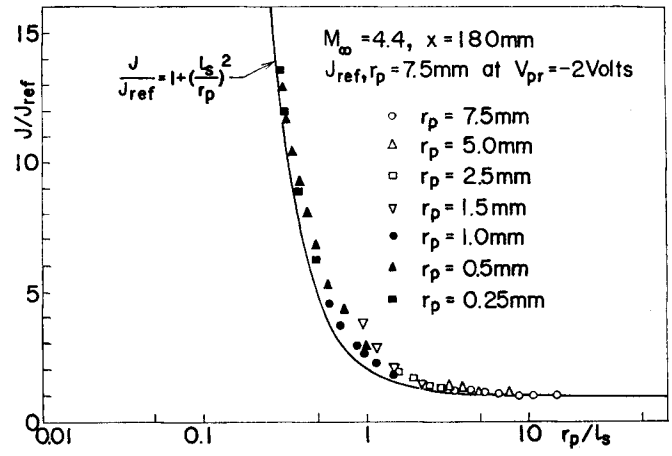

Fig. 11. Size Effect on Flush Probe Ion Current Collection at x=180mm.

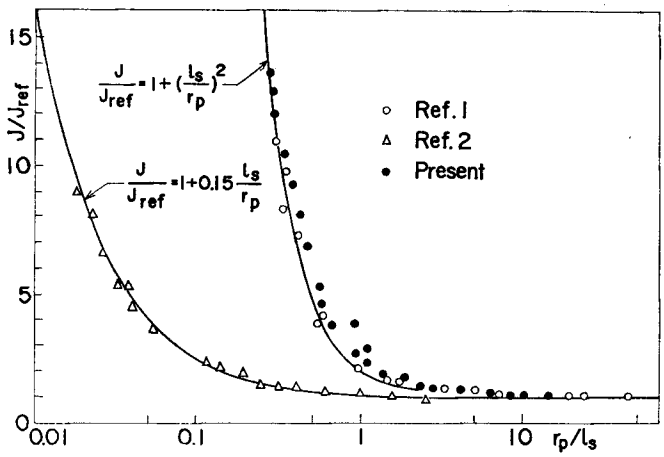

Fig. 12. Size Effect on Flush Probe Ion Current Collection.

density collections. Here the ion current density as a function of the ion number density at the outer edge of the boundary layer is calculated using Chung's relation:[13]

$$J=eD_a\left(\frac{\partial n_I}{\partial y}\right). \tag{26}$$

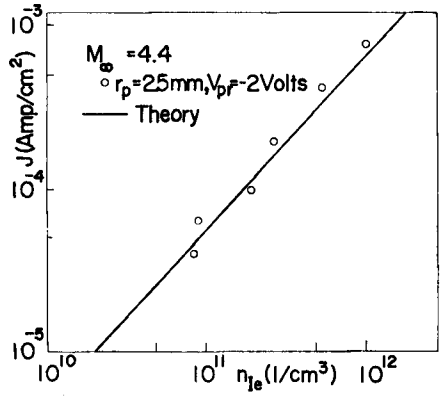

Fig. 13. Comparison of Experim ental and Theoretical Current Density Collection.

The actual ion current densities measured by means of the flush probes are then plotted as a function of the ion number density at the outer edge of the boundary layer. The data obtained with -2 volts biases seem to agree with the ion number densities calculated by using Chung's relation.

Figure14 shows the dimensionless probe area for $V_p=-2$ volts and $V_p=-8$ volts with the constant probe radius, $r_p=0.25$ mm. It is seen that the collected ion current density

decreases with an increase in the collecting probe area, and it approaches the constant value. It can be easily explained by considering the effect of sheath fringing field.

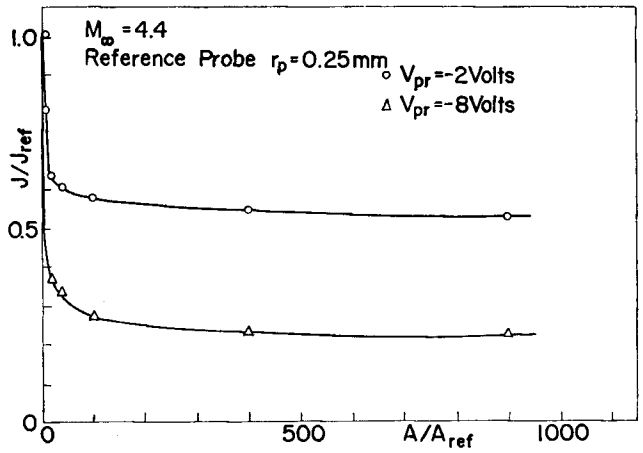

Fig. 14. Area Effect on Collected Current Density.

7. Conclusions

The appication of cylindrical probes and flush probes to the study of charged particle properties in the flat plate boundary layer of a partially ionized argon has been considered. Numerical results for the charged particle profiles in the quasi-neutral region of a flat plate boundary layer were also presented. On the basis of these experimental and numerical results, the following conclusions have been reached:

(1) The measured electron temperature and ion number density profiles in the flat plate boundary layer ared in good agreement with the calculated ones.

(2) The saturation ion current traces for the large-sized flush probes are essentially constant with respec to the biased potential. However, for the small-sized flush probes, the ion current is a very strong function of the biased potential.

(3) The measured ion current density appears to agree with $J/J_{ref}=1+(l_s/r_p)^2$, which is obtained from the free fall sheath consideration.

(4) The ion saturation current measured by means of flush probe can be used to predict n_{Te} with good accuracy by using the boundary layer theory.

(5) The collected ion current density decreases with an increase in the collecting probe area.

References

1) Tseng, R. C. and Talbot, L., AIAA Paper, No. 70-86 (1970); also AIAA J., Vol. 9 (1971), 1365.
2) Boyer, D. W. and Touryan, K. J., AIAA J., Vol. 10 (1972), 1667.
3) Lederman, S. and Avidor, J., Israel Journal of Technology, Vol. 9 (1971), 19.
4) Jaffrin, M. Y., Phys. Fluids, Vol. 8 (1965), 606.
5) Spitzer, L., Jr., Physics of Fully Ionized Gases, (1956), 72, Interscience.
6) Chen, C. J., J. Chem. Phys., Vol. 50 (1969), 1560.
7) Talbot, L., Chou, Y. S. and Roben, F., Institute of Engineering Research, University of California, Berkeley, Report, No. AS-65-14 (1965).
8) Chen, C. J., Phys. Rev., Vol. 163 (1967), 1.
9) Nishida, M. and Matsuoka, K., AIAA J., Vol. 9 (1971), 2117.
10) Sonin, A. A., Institute for Aerospace Studies, Toronto University, UTIAS Report, No. 109 (1965).
11) Kamimoto, G., Kimura, T. and Teshima, K., Dept. of Aero. Eng., Kyoto Univ., C.P. No. 7 (1965).
12) Brown, S. C., Introduction to Electrical Discharge in Gases, (1966), J. Wiley and Sons.
13) Chung, P. M., AIAA J., Vol. 3 (1965), 817.